

The structure of fluid trifluoromethane and methylfluoride

J. Neufeind ¹, H.E. Fischer ², W. Schröer ³

¹ Hamburger Synchrotronstrahlungslabor HASYLAB at DESY,
Notkestr 85, D-22603 Hamburg Germany

² Institut Laue-Langevin, 6 rue Jules Horowitz, BP 156, 38042
Grenoble Cedex 9, France †

³ Inst. f. Anorg. und Phys. Chem, Univ. Bremen, Leobener Str.
NW II, D-28359 Bremen, Germany

† present address: Laboratoire pour l'Utilisation du Rayonnement Electro-
magnétique (LURE), Centre Universitaire Paris-Sud, BP 34, 91898 ORSAY
cedex, France

Abstract. We present hard X-ray and neutron diffraction measurements on the polar fluorocarbons HCF₃ and H₃CF under supercritical conditions and for a range of molecular densities spanning about a factor of ten. The Levesque-Weiss-Reatto inversion scheme has been used to deduce the site-site potentials underlying the measured partial pair distribution functions. The orientational correlations between adjacent fluorocarbon molecules – which are characterized by quite large dipole moments but no tendency to form hydrogen bonds – are small compared to a highly polar system like fluid hydrogen chloride. In fact, the orientational correlations in HCF₃ and H₃CF are found to be nearly as small as those of fluid CF₄, a fluorocarbon with no dipole moment.

PACS: 61.20.Qg, 61.20.Ja, 61.25.Em

1. Introduction

The understanding of dielectric properties resulting from orientational correlations[1, 2], as well as the determination of orientational correlations from diffraction experiments[3, 4], are long standing problems in the physics of molecular fluids. The simple fluorocarbons HCF₃ and H₃CF are very interesting model substances in this context, as they possess rather large dipole moments ($1.65 \cdot 3.336 \cdot 10^{-30}\text{Cm}$), in the case of trifluoromethane – the same as that of the water molecule) but no tendency to form hydrogen bonds [5]. The investigation of the structure of the simple fluorocarbons H₃CF and HCF₃ thus enables the study of the structural effect of the molecular dipole alone.

Although the properties of these fluorocarbons are interesting, only very limited structural information is available so far. HCF₃ is discussed as replacement for chlorinated hydrocarbons as refrigerant since it has no ozone damaging effect, it has a shorter atmospheric lifetime and, hence, a lower global warming potential and it presents no toxicological risk [6, 7]. HCF₃ is discussed for extraction applications [8] and it has been shown, that the enantioselectivity of asymmetric catalysis can be controlled by the density of the fluoroform solvent [9]. The crystal structure of HCF₃ has been determined by a neutron powder diffraction experiment [10] and the molecular geometry by a gas phase electron diffraction

study [11]. The only fluorocarbon investigated in the supercritical regime is tetrafluoromethane[12], whereas deuterated trifluoromethane has been investigated in the liquid regime [13, 14]. In both cases the total neutron structure factor has been determined. References to the simulation studies performed for HCF_3 can be found in the recent work by Hloucha *et al* [15] beginning with the early work of Böhm *et al* [16].

The method used here to deduce molecular orientations is based on the potential inversion scheme of Levesque, Weis and Reatto [17]. From the result of hard X-ray and neutron diffraction experiments with isotopic substitution (NDIS) a site-site potential is deduced, which in turn can be used in a NVT-Monte-Carlo simulation to obtain the orientational correlations. The determination of the potential is facilitated by the ease with which the density of these systems can be varied, both having a critical point at about room temperature.

2. Experimental

We have investigated the structure of the fluid fluorocarbons in a range of pressures (28-100 bar) and temperatures (298-333 K) around the critical points of 58 bar, 317.8 K for H_3CF and 48.3 bar, 299.1 K for HCF_3 [18]. It was aimed to combine the information of a NDIS experiment [19, 20] and a hard X-ray diffraction experiment [21]. The neutron and hard X-ray experiments were both carried out using the same sample environment (Fig. 1) built especially for this experiment. The mechanical requirements of the pressure cell are moderate, and aluminum is a very suitable material for the sample container. Aluminum has a quite low scattering power for both neutrons and X-rays, only few powder lines due to its cubic structure and shows only little activation in a neutron beam. The samples, DCF_3 (98% D, Cambridge isotopes), HCF_3 , a 1:1 mixture $\text{HCF}_3/\text{DCF}_3$ and H_3CF (all Linde technical gases) can be condensed into the sample container through immersion in liquid nitrogen. The cell is then mounted inside a vacuum tank of the neutron or hard X-ray diffractometer. The sample pressure inside the mounted cell can be varied via an inert gas line, separated by a steel bellow from the sample. The temperature can be varied with a small heater at the bottom of the cell. The price of the deuterated gases requires the reduction of dead volumes inside the cell: The cell can be filled with ~ 4 g sample.

Figure 1. Schematic drawing and picture of the pressure set-up
A: sample container, B: steel bellow, C: pressure sensor, D: heater, E: temperature sensor, F: vent for the pressurizing medium, G: sample vent.

The neutron diffraction measurements were performed at the diffractometer D4b[22] at the ILL reactor source in Grenoble, using a wavelength of 0.7501 Å. Representative examples of the raw data are shown in Fig. 2, showing that the aluminum cell is clearly a viable alternative to the more usual vanadium and titanium-zirconium cells. The hard X-ray diffraction was performed at the high energy beamline BW5 at the DORIS storage ring at HASYLAB, Hamburg in its set-up for liquid and amorphous substances [23], using a wavelength of 0.1282 Å

3. Data analysis

The data were corrected for systematic effects like detector dead time, absorption, container scattering, multiple and incoherent scattering, using the procedure described in some detail in [24], and then normalized. The differential cross sections are expressed in terms of the scattering functions $S^{(x)}(Q)$ and $S^{(n)}(Q)$ for the hard X-ray and the neutron cases

$$S^{(n)}(Q) = \frac{\left(\frac{d\sigma}{d\Omega}\right)^{(n)} - \sum_i^{N_{uc}} \nu_i b_i^2}{\left(\sum_i^{N_{uc}} \nu_i b_i\right)^2} + 1 \quad (1)$$

$$S^{(x)}(Q) = i(Q) + 1 = \frac{\left(\frac{d\sigma}{d\Omega}\right)^{(x)} / \sigma_{el} - \sum_i^{N_{uc}} \nu_i f_i^2}{\left(\sum_i^{N_{uc}} \nu_i f_i\right)^2} + 1 \quad (2)$$

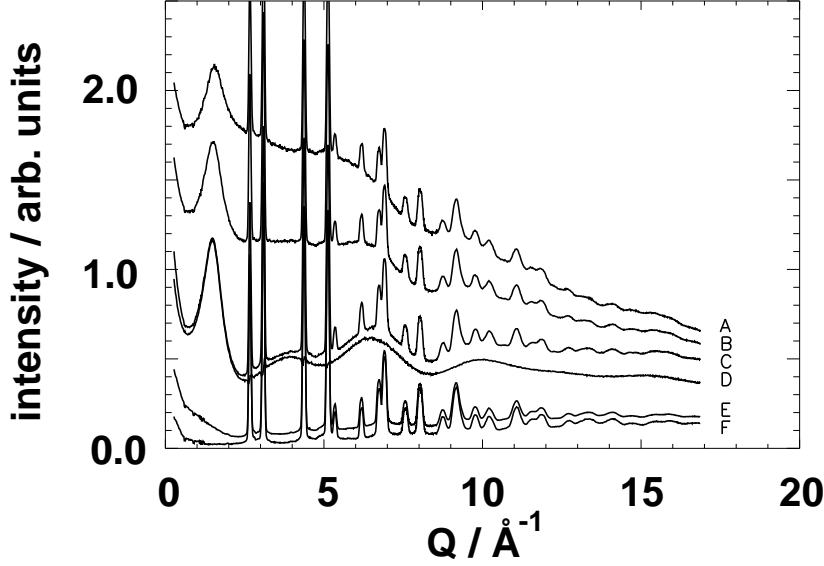


Figure 2. Raw data of the neutron diffraction experiment on trifluoromethane at D4b. .
A-C: Sample + cell scattering intensity of HCF_3 , MCF_3 (the H/D mixture) and DCF_3 respectively at liquid-like densities (30 °C, 100 bar), D: scattering intensity of C after subtraction of the cell scattering, E: Sample + cell scattering intensity of DCF_3 at gas-like densities (60 °C, 32 bar), F: empty aluminum container.

where $(\frac{d\sigma}{d\Omega})$ is the coherent differential cross section, b_i the coherent scattering lengths [25], f_i the X-ray form factors in the independent atom approximation [26], σ_{el} the scattering cross section of the free electron, ν_i the stoichiometric coefficient of the atom i , and where the sums are extending over the number of distinct atoms in the molecule N_{uc} , the subscript uc referring to the unit of composition, the molecule. In Fig. 3 the density dependence of the X-ray structure function of H_3CF is shown. Beyond $Q \sim 2.5 \text{ \AA}^{-1}$ the interference scattering intensity is dominated by the intramolecular contributions. Fitting of the Debye equation in the range $[4 < Q < Q_{max}]$:

$$i(Q)_{\text{intra}} = \sum_{i \neq j} 2 \frac{f_i f_j}{(\sum_i^{N_{uc}} \nu_i f_i)^2} \frac{\sin(Qr_{ij,eq})}{Qr_{ij,eq}} \exp(-Q^2 \gamma_{ij}^2 / 2.), \quad (3)$$

with $r_{ij,eq}$ the equilibrium distance of the atoms i and j within the molecule and γ_{ij} the displacement parameter, leads to $r_{\text{CF}} = 1.416(8) \text{ \AA}$ and $\gamma_{\text{CF}} = 0.050(18) \text{ \AA}$ independent of density. Likewise, the molecular parameters of trifluoromethane were determined and are shown in Table 1. For trifluoromethane the molecular parameters are also independent of the density and in excellent agreement with the gas phase values from ref. [11]. For the remainder of the article only the intermolecular contributions to the structure are considered.

The intermolecular scattering contribution is related to the weighted intermolecular pair distribution functions by a Fourier-sine transformation:

$$r \cdot (g^{(n)} - 1) = \frac{1}{2\pi^2 \rho_{uc}} \int Q \cdot (S^{(n)} - 1) \sin(Qr) dQ \quad (4)$$

$$r \cdot (g^{(x)} - 1) = \frac{1}{2\pi^2 \rho_{uc}} \int Q \cdot i(Q) \sin(Qr) dQ. \quad (5)$$

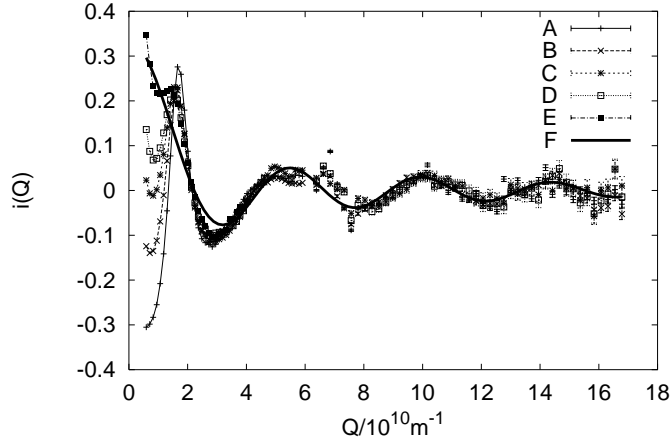


Figure 3. X-ray structure function $i(Q)$ of H_3CF at various densities. A: $\rho_{uc} = 17.6 \cdot 10^{-3} \text{ \AA}^{-3}$, B: $\rho_{uc} = 13.0 \cdot 10^{-3} \text{ \AA}^{-3}$, C: $\rho_{uc} = 10.4 \cdot 10^{-3} \text{ \AA}^{-3}$, D: $\rho_{uc} = 7.3 \cdot 10^{-3} \text{ \AA}^{-3}$, E: $\rho_{uc} = 2.6 \cdot 10^{-3} \text{ \AA}^{-3}$, F: Fit of equation 3 to the data with $r_{\text{CF}} = 1.416(8) \text{ \AA}$ and $\gamma_{\text{CF}} = 0.050(18) \text{ \AA}$.

where ρ_{uc} is the density per unit of composition (molecule). $g^{(x)}$ and $g^{(n)}$ and are weighted sums of the partial (site-site) pair distribution functions (PPDF):

$$g^{(n)} = \sum_{ij} w_{ij} g_{ij} \quad \text{with} \quad w_{ij} = \frac{\nu_i \nu_j b_i b_j}{(\sum_i \nu_i b_i)^2} \quad (6)$$

and

$$g^{(x)} = \sum_{ij} \text{FT}[w_{ij}(Q)] \otimes g_{ij} \quad \text{with} \quad w_{ij}(Q) = \frac{\nu_i \nu_j f_i(Q) f_j(Q)}{(\sum_i \nu_i f_i)^2}, \quad (7)$$

where $\text{FT}()$ is the Fourier sine transformation and \otimes the convolution operation.

Trifluoromethane has six PPDF, and four independent diffraction experiments were carried out. Consequently, assuming the independence of the structure from the isotopic composition, a set of one PPDF (HH) and three independent composite partial pair distribution functions (CPPDF) can be isolated, each of the CPPDF is the weighted sum of two PPDF. The three CPPDF are dominated by the fluorine PPDF, FF, FC and FH, while the carbon PPDF, CC and HC do contribute only very little. Alternatively the total pair distribution function can be split into HH, HX and XX CPPDF, with

	This work, fluid	crystal [10]	gas phase [11]
r_{CF}	1.327	1.315(4) ²	1.3284(31)
r_{FF}	2.153		
r_{HC}	1.088	1.111(7)	1.091(14)
r_{HF}	1.995		
γ_{CF}	.092		
γ_{FF}	0.104		
γ_{HC}	0.112		
γ_{HF}	0.145		
$\angle \text{HCF}$	111.0 ¹	109.77(32) ²	110.35
$\angle \text{FCF}$	108.4 ¹	109.14(43) ²	108.58(44)

Table 1. Molecular structure of HCF_3 .

All distances and displacement parameter in \AA , all angles in degree.

¹ The angles are not refined directly, but determined from the maxima of the distance distributions.

² Mean value of intramolecular distances and bond angles non equivalent in the crystal.

X either C or F. This is the same separation as that used in the case of the hydrogenhalides, with X=Cl in that case, thus enabling a proper comparison of our results with measurements of the structure of fluid HCl. All pair distribution functions are defined such that $\lim_{r \rightarrow \infty} g(r) = 1$.

4. Potential inversion

In order to generate a three dimensional picture of the structure from the pair distribution functions, the potential inversion scheme of Levesque, Weiss and Reatto [17] (LWR-scheme) was applied. The idea of this method is based on the equation:

$$g(r) = \exp \left[\frac{-v(r)}{kT} + g(r) - 1 - c(r) + B(r, v) \right] \quad (8)$$

relating the pair distribution function and the pair potential, where $v(r)$ is the pair potential, $c(r)$ the direct correlation function and $B(r, v)$ the bridge function. Starting with a first guess of the potential $v^{(1)}$, e.g. by neglecting the bridge function, a Monte Carlo simulation gives $g(r)^{(1)}$ and $c(r)^{(1)}$ belonging to $v^{(1)}$ and thus $B(r, v^{(1)})$. Substituting $B(r, v^{(n-1)})$ for $B(r, v)$ in equation 8 gives the LWR iteration formula

$$\begin{aligned} v^{(n)}/kT &= v^{(n-1)}/kT + \ln(g^{(n-1)}/g^{(exp)}) \\ &+ c^{(n-1)} - c^{(exp)} - g^{(n-1)} + g^{(exp)} \end{aligned} \quad (9)$$

Schommers [27] proposed a similar iteration scheme where only the logarithmic term of Eq. 9 is considered. Reatto *et al* have shown [28], that their algorithm converges - under certain conditions much - faster compared to the Schommers scheme. Soper's EPMC algorithm [29] uses the same iteration scheme as Schommers, but contrary to it is formulated for multi-element fluids. Likewise, it has been shown by Kahl and Kristufek [30] that the LWR scheme is applicable to polyatomic systems. The systems investigated here are even a step more complicated than the systems Kahl and Kristufek used, as the sites are connected by covalent bonds and the PPDF are not complete. Thus the HC and the CC site-site potentials were kept constant as hard sphere potentials. The method has already been tested under these conditions and compared to the results of Reverse Monte-Carlo (RMC) [31] simulations. A short account of the comparison between the potential inversion and the RMC method has been given elsewhere [32]. In the following only the results of the potential inversion method are given.

One test of the potential inversion scheme is the correct or incorrect prediction of the pair distribution function at several different state points from a pair potential determined at a specific state point. This is demonstrated in Fig. 4. This procedure also tests whether the intermolecular potential can be described as an effective two-body potential.

5. Results and discussion

In Fig. 4a the density dependence of $g_{XX}^{(n)}$ of trifluoromethane is shown. The density dependence of the other CPPDF is similar. At the higher densities $g_{XX}^{(n)}$ shows a typical liquid-like behavior and several maxima and minima. The maxima at larger distances die out when lowering the density, while the height of the first maximum increases. This is opposite to the behavior of fluid hydrogen chloride [34] or water [35] where the height of the main maximum decreases with density. The position of the main maximum remains almost unchanged.

The HCF₃ molecular potential has been determined as a site-site potential, whereas for H₃CF only the X-ray weighted pair distribution function $g(r)^{(x)}$ was determined, and thus an independent determination of H₃CF site-site potentials was not possible. The question arises as to whether the HCF₃ site-site potentials can also be used to describe the H₃CF structure, i.e. if these potentials have a general applicability to all fluorocarbons. Figure 5 indicates that the site-site potentials are indeed transferable to a different molecular species.

Density dependence of $g_{XX}^{(n)}$

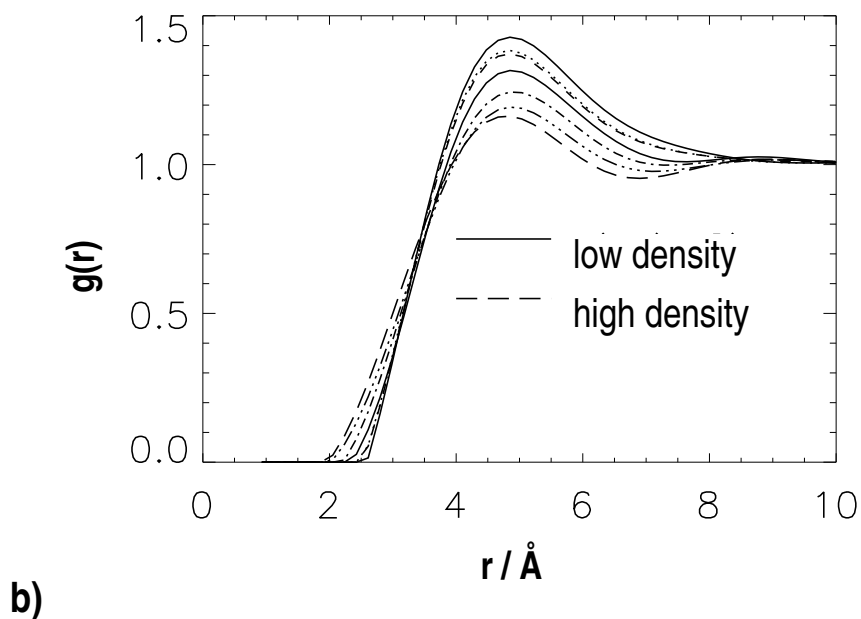
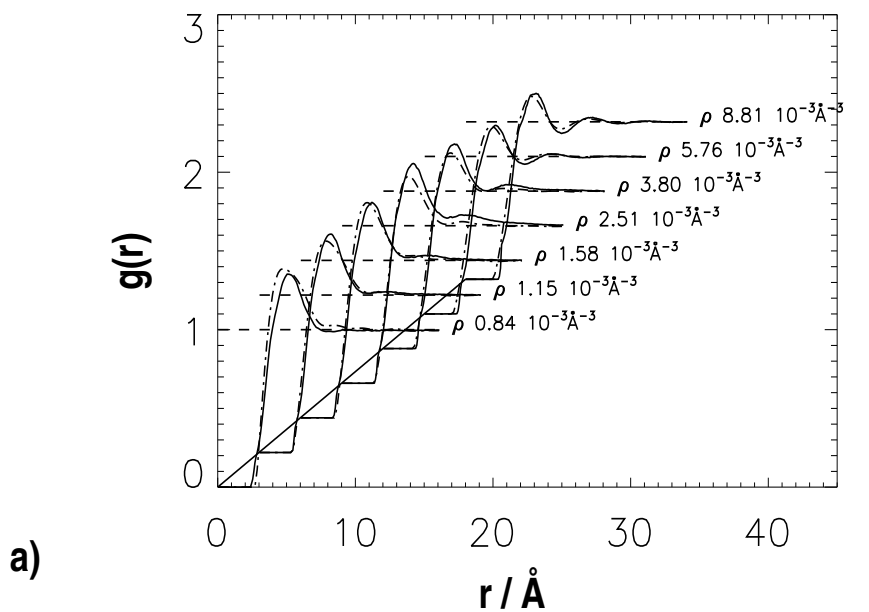


Figure 4. a) Example of the density dependence of the intermolecular part of the $g_{XX}^{(n)}$ CPPDF of HCF_3 . The experimental $g_{XX}^{(n)}$ is compared with the prediction of a potential model derived at some specific state point (f: $\rho_{uc} = 1.15 \cdot 10^{-3} \text{ \AA}^{-3}$).

b) Direct comparison of the experimental $g_{XX}^{(n)}$ at decreasing density. (same state points as in a)

The densities in the figure correspond to the following experimental conditions (from high to low density): a: $p=100 \text{ bar}$, $T=298\text{K}$, $\rho_{uc} = 8.8 \cdot 10^{-3} \text{ \AA}^{-3}$, b: $p=100 \text{ bar}$, $T=333\text{K}$, $\rho_{uc} = 5.8 \cdot 10^{-3} \text{ \AA}^{-3}$, c: $p=80 \text{ bar}$, $T=333\text{K}$, $\rho_{uc} = 3.8 \cdot 10^{-3} \text{ \AA}^{-3}$, d: $p=60 \text{ bar}$, $T=333\text{K}$, $\rho_{uc} = 2.5 \cdot 10^{-3} \text{ \AA}^{-3}$, e: $p=50 \text{ bar}$, $T=333\text{K}$, $\rho_{uc} = 1.6 \cdot 10^{-3} \text{ \AA}^{-3}$, f: $p=40 \text{ bar}$, $T=333\text{K}$, $\rho_{uc} = 1.15 \cdot 10^{-3} \text{ \AA}^{-3}$, g: $p=32 \text{ bar}$, $T=333\text{K}$, $\rho_{uc} = 0.84 \cdot 10^{-3} \text{ \AA}^{-3}$.

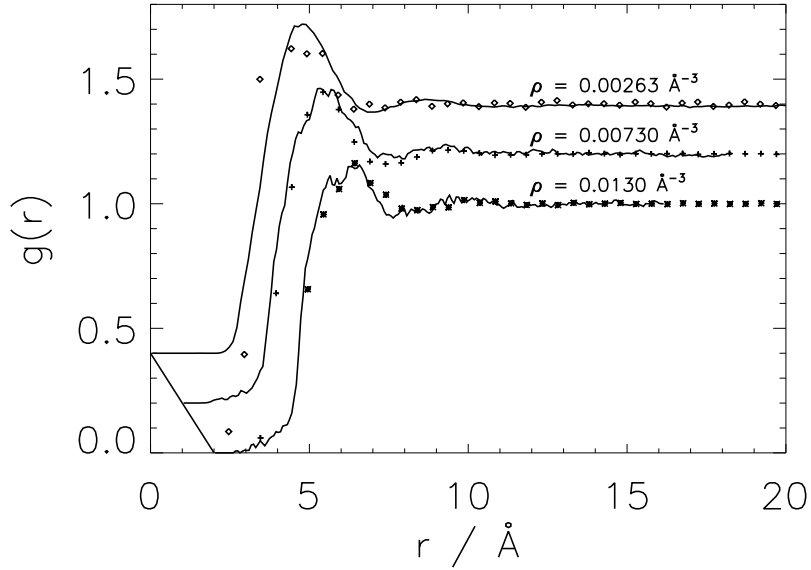


Figure 5. Comparison of $g^{(x)}(r)$ for H_3CF from the experiment with the result from a Monte-Carlo simulation using the site-site potentials derived for HCF_3 . The symbols correspond to the experimental $g^{(x)}(r)$, the separation of the symbols in x-direction corresponds to the experimental resolution, the solid line to the simulation. The $g^{(x)}(r)$ correspond to different densities shown in the figure (state point B, D and E in Fig. 3).

The aim of the present work was to determine the influence of the molecular dipole on the orientational correlations between the molecules. Fig. 6 compares the HH, HX and XX pair distribution functions of fluid HCl [34], HCF_3 and H_3CF . The three PPDF of HCl are quite structured and dissimilar while the corresponding CPPDF of both HCF_3 and H_3CF are much less structured and very similar. This behavior is an indication that there will be no strong preference for particular orientations in the fluorocarbons. The most remarkable difference can be seen in the XX-(C)PPDF: g_{ClCl} in HCl has the highest maximum.

Fig. 7 quantifies this qualitative statement and shows $P(r_{\text{COM}}, \cos(\theta))$, the relative probability of finding a second molecule at the center of mass distance r_{COM} in an orientation $\cos(\theta)$, where θ is the angle between the molecular dipoles. This figure is to be compared to figures 5 and 7 of Ref. [34] and to figure 9 of Ref. [12]. While the first work determines the orientational correlation in fluid HCl via the EPMC formalism (truncated version of Eq. 9) and finds pronounced orientational correlations, the second is a Reverse Monte-Carlo study using a total neutron structure factor measurement of fluid CF_4 as input and finds a $P(r_{\text{COM}}, \theta)$ very similar to fig. 7, structured only at very short distances.

Averaging the mean $\langle \cos(\theta) \rangle_r$ via

$$g_K = 1 + \int_0^\infty N(r) \langle \cos(\theta) \rangle_r dr \quad (10)$$

with $N(r) = 4\pi\rho_{uc}r^2g_{\text{COM}}$, to yield a Kirkwood g-factor leads to values very close to one (0.995 on average) in the entire density range investigated for both HCF_3 and H_3CF . This is in agreement with advanced theories of the dielectric properties of these materials [33].

The largely simplified model illustrated in Fig. 8a can help to understand this behavior. At a distance of 5\AA , the maximum of the pair distribution functions of HCF_3 , the energy difference between parallel and antiparallel alignment of point dipoles of $1.65 \cdot 3.336 \cdot 10^{-30}$ Cm located at the center of mass is about 2kT for the polar positions and about 1kT for the equatorial positions. In a two level system this would

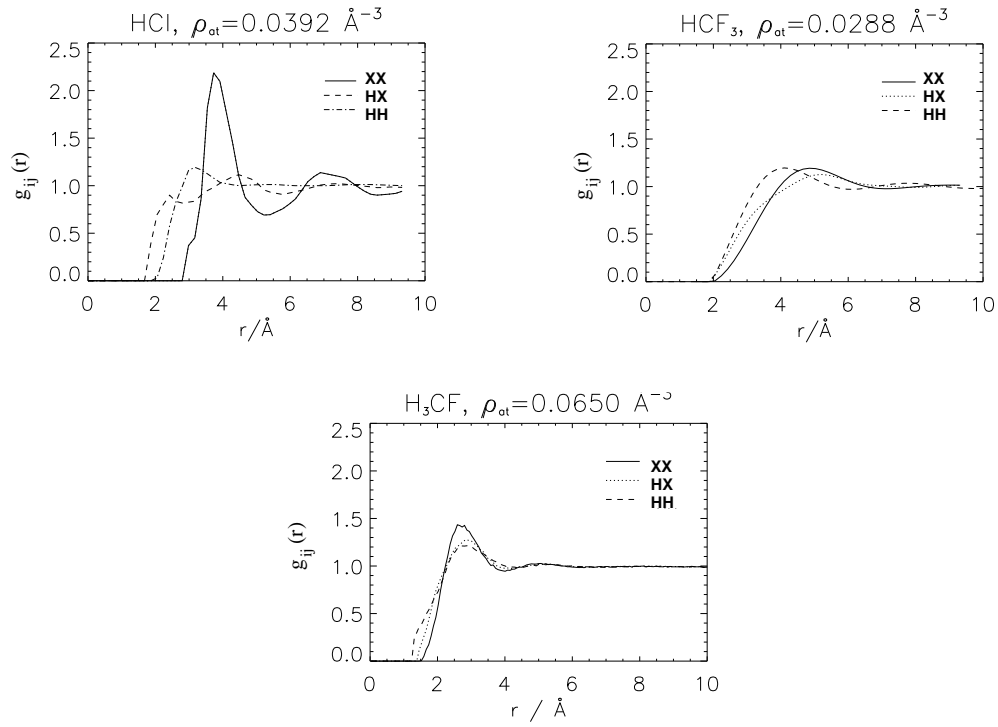


Figure 6. Comparison of the HH, HX and XX CPPDF of HCF_3 and H_3CF with the PPDF of HCl [34]. The CPPDF for H_3CF are simulation results

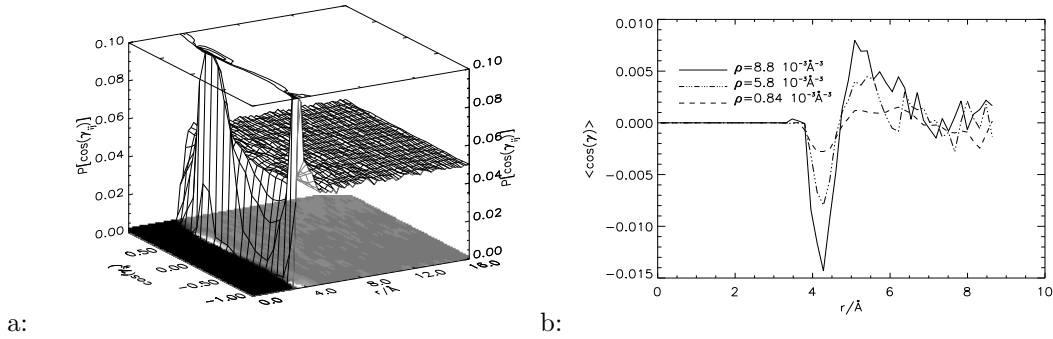


Figure 7. a: Cosine distribution of the angle θ between the molecular dipoles of HCF_3 at $\rho=8.8 \cdot 10^{-3} \text{Å}^{-3}$,
b: Mean cosine of the angle θ versus the center of mass distance at three different densities.

lead to seven times more parallel than antiparallel orientation in polar positions and three times more antiparallel orientation in equatorial positions. But the equatorial region is four times larger, leading to an almost complete cancelation of parallel and antiparallel orientations.

For HCl a preference for a polar arrangement of molecules has been found [34] (molecules directly 'below' or 'on top' of each other referred to the direction of the dipole). For these molecules in polar arrangement a strong preference for parallel orientations has been found - up to 17 times more parallel orientated dipoles than expected from a random distribution. The cosine distribution to be expected for point dipoles in a polar arrangement is:

$$P[r, \cos(\theta)] = \frac{\exp[k(r) \cos(\theta)]}{\int_{-1}^1 \exp[k(r) \cos(\theta)] d \cos \theta} \quad (11)$$

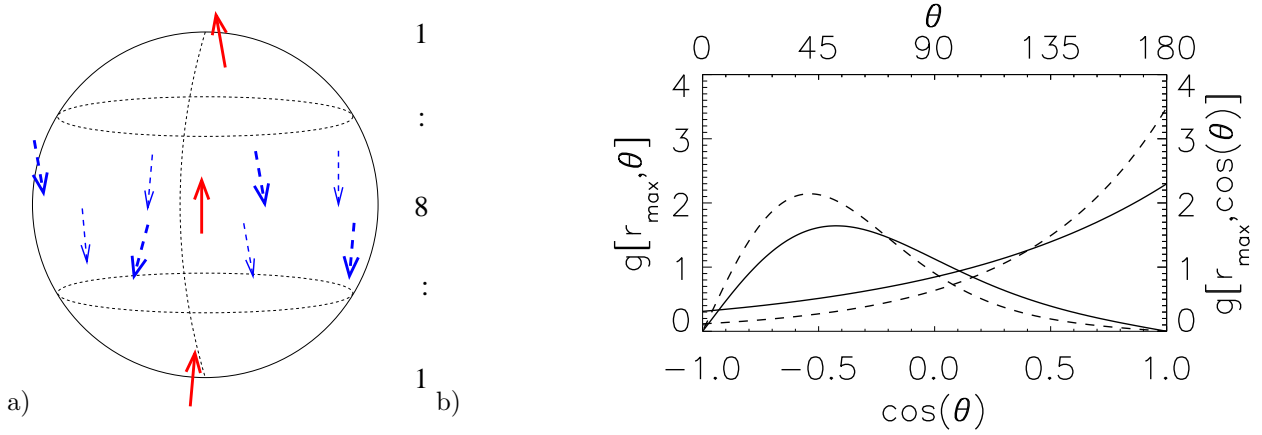


Figure 8. a) Simplified model of the relative orientation of dipolar molecules. Explanation in the text. b) Cosine distribution and theta distribution to be expected from two point dipoles in polar arrangement for $p = 1.65 \cdot 3.336 \cdot 10^{-30}$ Cm, $r_{\max} = 5 \text{ \AA}$ (HCF₃, solid line) and $p = 1.07 \cdot 3.336 \cdot 10^{-30}$ Cm, $r_{\max} = 3.6 \text{ \AA}$ (HCl, broken line)

with $k(r) = 2 \cdot p^2 / 4\pi\epsilon r^3$. This function is shown for $r = r_{\max}$, with r_{\max} the first maximum of $g(r_{COM})$ in Fig. 8b. With $p = 1.07 \cdot 3.336 \cdot 10^{-30}$ Cm [36] and $r_{\max} = 3.6 \text{ \AA}$ thus only 3.5 time more parallel oriented dipoles as in a random distribution should be found. From a simple point dipole model a less pronounced preference of parallel orientation as found by [34] is predicted for HCl, while on the other hand from this model a stronger preference than actually found would be expected for both, HCF₃ and H₃CF, probably due to the detailed molecular geometry and specific site-site interactions. These two effects, the cancelation of parallel and anti-parallel orientations and specific site-site interactions lead finally to the average behavior shown in Fig. 7 very similar to fluid CF₄.

Hloucha *et al.* [15] recently published a constant NPT Monte-Carlo simulation of liquid HCF₃ at subcritical temperatures. Their model is a rigid five site model, with a Lennard-Jones contribution, partial charges at the sites and point dipoles at the center of mass, with a constant and an induced contribution. With this model and in the dense liquid more pronounced orientational correlations between neighboring molecules as in this work are found. The positive peak in $\langle \cos(\theta) \rangle_r$ at $r \sim 4.5 \text{ \AA}$ in Fig. 7 is higher by a factor of two and the negative peak at close contact is missing. Hloucha *et al.* observed a decreasing trend in the orientational order with decreasing density which will tend to level out the differences in orientational order in the range of densities investigated here. Although the detailed comparison is complicated by the difference in the range of thermodynamic parameters investigated, this is supporting the point of view that the orientational ordering in HCF₃ is even less pronounced than predicted by a dipolar picture.

The spatial arrangement of neighboring molecules is illustrated in Fig. 9 which compares the crystal (a) – the positional parameters are taken from [10] – and the fluid at liquid like densities (b). In the crystal each trifluoromethane molecule is surrounded by twelve neighboring molecules at nearly the same distance. Among these, two are oriented parallel and two antiparallel, the remaining two times four molecules in two different T-orientations, that are orientations where the dipole moments are perpendicular to each other. Fig. 9b is a snap-shot of a simulation at $\rho_{uc} = 0.0088 \text{ \AA}^{-3}$. Again, the twelve next-neighbors are shown. The orientation of these molecules has been grouped into four classes having a $\cos(\theta)$ between -1.0 and -0.5, -0.5 and 0.0, 0.0 and 0.5 and 0.5 and 1.0, respectively, with θ the angle between the molecular dipoles. Again, quasi T-orientations occur more often. In the fluid this snap-shot is only representative

of course, the ensemble of structures leads to Fig. 7.

Figure 9. Relative orientation of next-neighbor molecules in crystalline HCF_3 (a) and dense fluid HCF_3 (b).

The relative orientation to the central molecule is indicated with a color code. In the crystal: Red (R): parallel, green (G) antiparallel, blue (B) and black (b): different T-configurations. In the fluid: red $1.0 > \cos(\theta) > 0.5$, blue $0.5 > \cos(\theta) > 0$, green $0 > \cos(\theta) > -0.5$, black $-0.5 > \cos(\theta) > -1.0$.

6. Conclusion

The density dependence of orientational correlations in fluid trifluoromethane and methylfluoride has been studied by NVT-Monte-Carlo simulations using effective site-site two body potentials derived via the Levesque-Weis-Reatto inversion scheme from NDIS and hard X-ray diffraction data of fluid trifluoromethane. Advanced theories of the dielectric properties of these materials predict a Kirkwood-g-factor close to one in the entire density range investigated here. The orientational correlations found in the simulation are in full agreement with this prediction. Detailed comparison with the orientational correlations found in fluid hydrogenchloride and tetrafluoromethane shows that the orientational correlation in HCF_3 and H_3CF are closer to tetrafluoromethane than to hydrogenchloride, although the interaction energy of the molecular dipoles is comparable to HCl in these systems. This and the comparison with the simulation results for a dipolar model of HCF_3 suggests that in the fluorocarbons site specific interaction results in weaker orientational correlations than predicted by a dipolar model while in fluid HCl the orientational ordering is enhanced.

7. Acknowledgment

The assistance of P. Palleau and O. Koch during the neutron experiment and the help of A. Swiderski in constructing the pressure cell is gratefully acknowledged.

- [1] Buckingham, A. D., 1967, *Adv. Chem. Phys.* **12** 107
- [2] Schröer, W., 1985, *Adv. Chem. Phys.*, **63** 719
- [3] Zeidler, M. D., 1982, *Z. f. phys. Chem. NF* **133** 1
- [4] Soper, A. K., Andreani, C., Nardone, M. 1994, *Phys. Rev. E* **47** 2598
- [5] Reuter, K., Rosenzweig, S., Franck, E. U., 1989, *Physica A* **156** 294
- [6] Pires, P. F., Guedes, H. J. R., 1999, *J. Chem. Thermodynamics*, **31** 479
- [7] Fermiglia, M., Priel, S., 1999, *Fluid Phase Equil.* **166** 21
- [8] Zhao, J., Olesik, S. V., 1999, *Fluid Phase Equil.* **154** 261
- [9] Wynne, D. C., Jessop, Ph. G., 1999, *Angew. Chem. Int. Ed.* **38** 1143
- [10] Torrie, B. H., Binbrek, O. S., Powell, B. M., 1996, *Molec. Phys.* **87** 1007
- [11] Kawashina, Y., Cox, A. P., 1978, *J. Molec. Spectrosc.* **72**, 423
- [12] Waldner, I., Bassen, A., Bertagnolli, H., Tödheide, K., Strauss, G., Soper, A. K., 1997, *J. Chem. Phys.* **107** 10667
- [13] Mort, K. A., Johnson, K. A., Cooper, D. L., Burgess, A. N., Howells, W. S., 1997, *Molec. Phys.*, **90** 415
- [14] Hall, C. D., Johnson, K. A., Burgess, A. N., Winterton, N., Howells, W. S., 1991, *Molec. Phys.* **74** 27
- [15] Hloucha, M., Deiters, U. K., 1998, *Fluid Phase Equil.* **149** 41
- [16] Böhm, H. J., Meissner, C., Ahlrichs, C. J., 1984, *Molec. Phys.* **53** 651
- [17] Levesque, D., Weis, J. J., Reatto, L. 1985, *Phys. Rev. Lett.* **54** 451
- [18] Lide, D. R. (ed.), 1998, *CRC Handbook of Chemistry and Physics* (CRC Press: Boca Raton)
- [19] Enderby, J. E., North, D. M., Egelstaff, P. A., 1966 *Philos. Mag.* **14** 961
- [20] Suck, J. B., Raoux, D., Chieux, P., Riekkel, C. (eds.), 1992, *Methods in the Determination of Partial Structure Factors of Disordered Matter by Neutron and Anomalous X-Ray Diffraction* (World Scientific: Singapur)
- [21] Poulsen, H. F., Neuefeind, J., Neumann, H.-B., Schneider, J. R., Zeidler, M. D., 1995, *J. Non-Cryst. Sol.* **188** 63
- [22] Ibel, K. (ed.), 1994, *Guide to Neutron Research Facilities at the ILL* (ILL: Grenoble)
- [23] Bouchard, R., Hupfeld, D., Lippmann, T., Neuefeind, J., Neumann, H.-B., Poulsen, H. F., Rütt, U., Schneider, J. R., Süßenbach, J., v. Zimmermann, M., 1998, *J. Synchrotron Rad.* **5**, 90
- [24] Weitkamp, T. Neuefeind, J., Fischer, H. E., Zeidler, M. D., 2000, *Molec. Phys.*, **98**, 125
- [25] Köster, L., Rauch, H., Seymann, E., 1991 *At. Data Nucl. Data Tab.* **49**, 65
- [26] J. H. Hubell, W. J. Veigele, E. A. Briggs, R. T. Brown, D. T. Cromer, R. J. Howerton, 1995, *J. Phys. Chem. Ref. Data* **4** 471
- [27] Schommers, W., 1983, *Phys. Rev. A* **28**, 3599
- [28] Reatto, L., Levesque, D., Weis, J. J., 1986, *Phys. Rev. A*, **33** 3451
- [29] Soper, A. K., 1996, *Chem. Phys.* **202**, 295

- [30] Kahl, G., Kristufek, K., 1994 Phys. Rev. E, **49**, 3565
- [31] McGreevy, R. L., Pusztai, L., 1988, Mol. Sim. **1** 359
- [32] Neufeind, J., Fischer, H. E., Schröer, W., 2000, Physica B, **276-278** 481
- [33] Schröer, W., Labrenz, D., Rybarsch, C. in Dorfmueller, Th. (ed.), 1989, *Reactive and Flexible Molecules in Liquids* (Kluwer: Deventer) 141
- [34] Andreani, C., Ricci, M. A., Nardone, M., Ricci, F. P. Soper, A. K., 1997, J. Chem. Phys. **107** ,214
- [35] Soper, A. K., Bruni, F. , Ricci, M. A. , 1997, J. Chem. Phys. **106** ,247
- [36] Greenwood, N. N., Earnshaw, A., 1984, *Chemistry of the elements* (Pergamon: Oxford)

This figure "neu01.jpg" is available in "jpg" format from:

<http://arxiv.org/ps/cond-mat/0006157v1>

This figure "neu09.jpg" is available in "jpg" format from:

<http://arxiv.org/ps/cond-mat/0006157v1>